Journal of Luminescence 133 (2013) 10–14

Contents lists available at SciVerse ScienceDirect

Journal of Luminescence

journal homepage: www.elsevier.com/locate/jlumin

Raman laser cooling of solids

Stephen C. Rand *

Division of Applied Physics, University of Michigan, Ann Arbor, Michigan, USA

ARTICLE INFO

Available online 5 February 2012

Keywords:
Optical refrigeration

ABSTRACT

A new approach is proposed for 3-D laser cooling of solids. Stimulated Raman scattering on a narrowband electronic transition is used in conjunction with 1-photon optical pumping on a broadband transition to provide a mechanism that cools all the vibrational modes of solids while conserving energy and momentum, photon by photon. The individual steps in the 2-photon Raman process are 4f–5d and 5d–4f transitions which are electric-dipole-allowed (broadband) transitions that form a Λ-system. By contrast, the 2-photon transition between the 4f states of the rare earth ion is narrowband. By considering examples of Ce^{3+} ions in $Y_3Al_5O_{12}$ and CeF_3, elevated transition rates are predicted to offer substantial improvement over anti-Stokes fluorescence cooling when all 1-photon detunings exceed their corresponding Stokes shifts.

1. Introduction

Optical refrigeration of gases is a relatively mature subject. In the past, laser cooling of bosonic systems was systematically developed [1–3] to achieve Bose–Einstein Condensation (BEC) for the first time [4], and the continuing effort to refine techniques that allow light to transport energy, momentum, and entropy out of atomic systems has shown that fermionic atoms can similarly condense into a single macroscopic quantum state [5]. These advances have drawn the subjects of superconductivity and BEC closer together and promise a unified view of these basic physics topics in the future. Experimental techniques for laser cooling have relied heavily on one simple but important characteristic of atoms in gases, namely that the atoms comprising a gas are in motion. Moving atoms experience the Doppler effect in inelastic collisions with photons, and can progressively be slowed down (cooled) while conserving energy and momentum in each and every interaction, provided that the light field undergoes an increase of entropy. Hence, although other mechanisms such as evaporative cooling have been applied in combination with laser cooling to attain the most extreme temperatures [4], it may be said that the harnessing of Doppler interactions has provided the most powerful set of approaches for optical cooling [6–10]. Unfortunately in solids the Doppler effect is ostensibly absent. This implies that the optical refrigeration of condensed matter must rely on a drastically more limited set of cooling mechanisms, and dims the prospect of using condensed matter to form new quantum states.

The motivation to discover efficient new laser cooling methods for condensed matter is nevertheless strong. Potential applications exist for "radiation-balanced" solid state lasers [11], improved gravitational wave detection [12], compact frequency references [13], refrigeration of infrared imagers below the thermo-electric limit in space [14], and compact cooling systems for super-conducting electronics. In the past, the axial vibrations of mirrors in Fabry–Perot interferometers were reduced with all-optical techniques to improve the sensitivity limits of gravitational observatories. However this opto-mechanical cooling of a single mode was not accompanied by an irreversible increase in entropy of the optical field and therefore altered the (non-equilibrium) distribution of phonons without cooling the solid as a whole. Parallel efforts with anti-Stokes cooling sought to cool the entire distribution of internal vibrational modes of solids in order to surpass the thermo-electric cooling limit that determines the signal-to-noise ratio of imaging arrays in space. Space-based infrared imagery is an example of an important technology that is hampered by detector noise, and could be greatly improved by refrigeration below this limit (N 153) in the rarified environment of space. Thermo-electric temperature limitations have now been surpassed with anti-Stokes fluorescence cooling [14], but far more effective methods are needed to reach temperatures of only a few Kelvin starting from room temperature. There is also interest in the fundamental objective of cooling solids to their vibrational ground state, but higher cooling rates are needed for that too.

In this paper, a new method is outlined that accelerates cooling of the internal vibrations of solids by combining a fast, stimulated Raman process to annihilate specific phonons of the host medium in a resonant manner with rapid optical pumping on an allowed fluorescent transition. The method avoids heating due to multi-phonon emission by atoms with arbitrarily large

* Tel.: +734 763 6810.
E-mail address: scr@umich.edu

0022-2313/$ - see front matter © 2012 Elsevier B.V. All rights reserved.
doi:10.1016/j.jlumin.2012.01.019

Stokes shifts (and high transition rates) and furnishes the necessary increase in entropy of the radiation field [15] to cool the entire solid.

2. "Doppler" cooling principle for solids

The vibrations of atoms or molecules in a solid constitute the motion that determines its kinetic temperature. This motion may be analyzed as phonons, and phonons undergo "collisions" during their interactions with light. As a consequence, incident photons of frequency and wavevector (ω_1,k_1) experience Doppler-like interactions with phonons of frequency and wavevector (Ω,q) to produce scattered light. The scattered field has a frequency and wavevector described by (ω_2,k_2), and the conditions $\omega_2=\omega_1\pm\Omega$ and $\overline{k}_2=\overline{k}_1\pm\overline{q}$ must be met to conserve energy and momentum when phonons are annihilated or created (upper or lower sign, respectively). Doppler analogies are commonplace in acousto-optics [10], but they take on special significance in the context of laser cooling of solids where they can guide the adaptation of Doppler-shifted atom-field interactions to phonon-field interactions in condensed matter.

Here we propose an approach to cool rare earth ions in solids based on a coherent 2-photon interaction [16–18] that destroys phonons and an incoherent step that adds entropy, completing a repetitive cooling cycle that exploits fast fluorescence of impurity or host ions. The method uses counter-propagating laser beams whose difference frequency is slightly lower than the transition frequency to a long-lived excited electronic state. A phonon is annihilated during each electronic Raman transition to the latter "shelving" state, when detuning is to the long wavelength ("red") side of the 2-photon $4f^n$–$4f^n$ transition. Subsequently, the excited ion is returned to its ground state via fast optical pumping on a spontaneous $4f^{n-1}\,5d\leftrightarrow 4f^n$ transition which raises the entropy of the field. This last step makes the cooling irreversible. Through rapid repetition of this phonon annihilation and optical pumping cycle, cooling can proceed at a high rate.

Fig. 1 illustrates the basic geometry of inelastic light scattering by phonons. In spontaneous 1-photon interactions, the scattered light has a higher or a lower optical frequency and wavevector $(\omega\pm\Omega,\ k\pm q)$ depending on whether the specific phonon that conserves energy and momentum at scattering angle θ is absorbed or emitted. Consequently, both upshifted and downshifted components are observed in the spontaneous light scattering spectrum. In scattering with two input fields however, interaction with a specific phonon may be made more selective, through the involvement of an excited state resonance. For example, counter-propagating beams with a positive 2-photon detuning of $\delta\equiv\Delta_F-(\omega_1-\omega_2)=\Omega$ in Ce^{3+} (with respect to the $^2F_{5/2}(n)\rightarrow{}^2F_{7/2}(n)$ transition, as shown in Fig. 2) can produce only phonon annihilation at frequency Ω through the vibronic transition $^2F_{5/2}(n)\rightarrow{}^2F_{7/2}(n-1)$. If the fields $\overline{E}_1$ and $\overline{E}_2$ are interchanged, a phonon of the same frequency propagating in the opposite direction can be annihilated. However no phonons are *created* by this process in either direction on average.

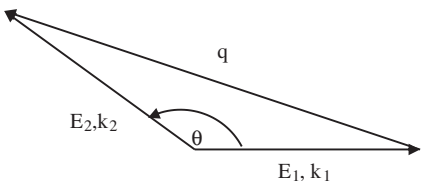

Fig. 1. Wavevector diagram for Raman scattering through angle θ. Phonon wavevector $\overline{q}=\overline{k}_2-\overline{k}_1$ conserves linear momentum of the vibrational mode driven by field $\overline{E}_1$ and field $\overline{E}_2$.

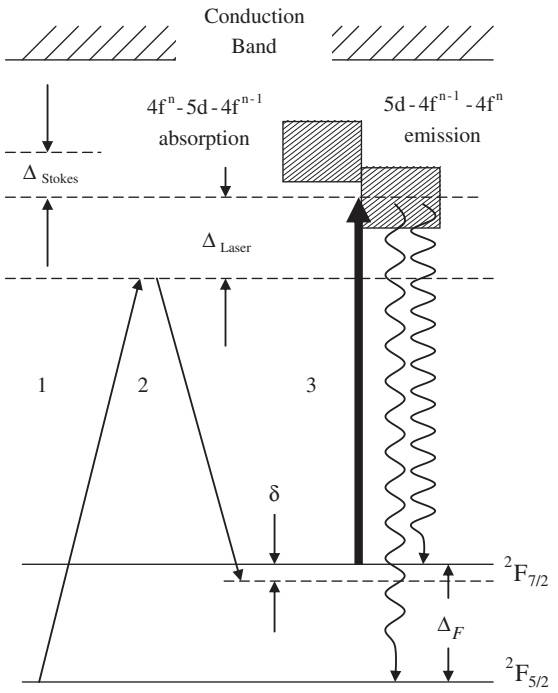

Fig. 2. Stimulated Raman cooling of Ce^{3+}. Fields 1 and 2 are applied simultaneously to cause the absorption of a phonon of wavevector $q\cong 2k$ and frequency $\Omega=\delta$. The bold vertical arrow (repump field 3 at ω_3) provides an optical pumping to avoid population buildup in the $^2F_{7/2}$ state that would reverse the 2-photon process. This field also ensures that entropy increases in the overall interaction [4].

Phonon annihilation cannot be sustained indefinitely using stimulated Raman scattering with continuous-wave radiation. Because the net Raman transition rate is proportional to the population difference between the $^2F_{5/2}$ and $^2F_{7/2}$ levels, forward and backward transitions are balanced at high intensity in steady-state. Under continuous excitation, the excited state population accumulates until it equals that of the ground state. Forward (cooling) and backward (heating) transition rates then become equal. To ensure that only the forward process takes place, the Raman interaction should be pulsed and the $^2F_{7/2}$ state must be emptied periodically. Depletion of the $^2F_{7/2}$ state can be accomplished with an intense "repump" field $\overline{E}_3$ of an appropriate wavelength, as depicted in Fig. 2.

The repump interaction at ω_3, as well as all other possible 1-photon transitions in the overall cooling cycle (namely those at ω_1 or ω_2), must avoid generating phonons originating from relaxation in either the ground or excited state. Transitions consistent with zero heating (or net cooling) require detuning to the red by an amount equal to or greater than the Stokes shift of the longest wavelength $4f^{n-1}\,5d\leftrightarrow 4f^n$ transition. For Ce^{3+} this means,

$$\Delta_{Laser}\geq\Delta_{Stokes}+\Delta_F \tag{1}$$

This choice is necessary to ensure that each photon has less energy than required to generate either a vibrationally excited upper state or a vibrationally excited ground state. The maximum 2-photon Raman transition probability compatible with cooling therefore occurs when $\Delta_{Laser}=\Delta_{Stokes}+\Delta_F$ in the Ce^{3+} system.

The inter-configurational transition of Ce^{3+} is of $5d\rightarrow 4f$ character, so the corresponding wavelength is strongly host-dependent. Consequently the selection of host crystal can in principle be used to match desirable laser wavelengths for cooling or optical pumping. On the other hand, an arbitrary choice of host does not change the fundamental design of the cooling

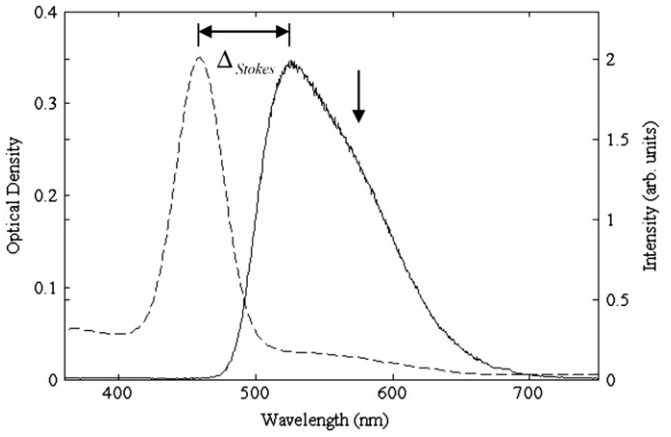

Fig. 3. Absorption (dashed) and emission (solid) curves of Ce:YAG. The vertical arrow indicates the peak of the $4f^{n-1}\ 5d \leftrightarrow {}^2F_{7/2}$ fluorescent transition which appears as a shoulder on the two overlapping inter-configurational transitions back to $4f^n$. This identifies the shortest wavelength excitation that can be used for Raman cooling of Ce:YAG.

experiment or alter the key conditions that determine optimal detunings for experiments. It is sufficient to measure the fluorescence emission spectrum of Ce^{3+} in the chosen host to determine the minimum 1-photon detunings compatible with overall cooling. This determination is illustrated for the case of Ce:YAG in Fig. 3. All incident laser light must have a wavelength longer than that of the fluorescent transition $4f^{n-1}\ 5d \leftrightarrow {}^2F_{7/2}$ in Ce^{3+}. In the figure, the minimum wavelength compatible with cooling in Ce:YAG is marked by the vertical arrow at the shoulder corresponding to this transition in the emission spectrum.

3. Results for the cooling rate

We now proceed to estimate the high temperature cooling rate by specializing to optical phonons in the classical limit. We omit the case of acoustic phonons since they couple to the light via deformation potential rather than transverse, field-driven charge motion [19].

For optimum efficiency in the stimulated Raman interaction, two separate detuning conditions must be met. The first is the 1-photon detuning: $\Delta_{Laser} \geq \Delta_{Stokes} + \Delta_F$. The second calls for a 2-photon detuning equal to the selected phonon frequency Ω, which could be an arbitrary value or the dominant phonon frequency Ω_{dom} at a temperature of interest ($\delta = \Omega_{dom}(T)$). The latter detuning not only ensures resonance with a selected vibronic transition, but also implies "adjustability" to adapt to temperature changes as the sample cools. By tuning the frequency offset of the counter-propagating Raman beams to match a specific phonon frequency and wavevector, energy and momentum can be conserved on average in each phonon annihilation. Additionally, the detuning can theoretically be adjusted to follow the shift in the distribution of phonon occupation probability, thereby maximizing the cooling rate at any given temperature. In this way the 2-photon detuning can be used to maintain resonance with a dominant phonon at frequency $\Omega_{\mathrm{dom}}\ (T)$ during cooling in the same way that chirped detuning is used during the laser cooling of gases to track the average Doppler shift [16,18]. However the fixed optical geometry and fixed wavevector difference of the optical waves mandate that changes in the detuning must be performed in jumps between discrete optical modes rather than as the continuous, monotonic adjustment that is typically used in laser cooling of gases.

For the present estimate the 2-photon detuning is assumed to have a fixed value $\delta = \Omega$ matching the frequency of the phonon of interest. The rate of energy loss R per coolant atom is then simply given by the stimulated Raman transition rate $\Gamma_R(\Delta_{Laser})$ to the excited state ${}^2F_{7/2}$ multiplied by the phonon energy. That is,

$$R = \Gamma_R(\Delta_{Laser})\hbar\Omega \tag{2}$$

In the model system based on Ce^{3+} and depicted in Fig. 2, there are only three active levels to take into account, namely the high-lying 5d state and the two lower levels of the $4f^n$ configuration. We refer to ${}^2F_{5/2}(n)$ and ${}^2F_{7/2}(n-1)$ as states 1 and 3, respectively, and the excited state of the $4f^{n-1}$ 5d configuration is labeled as 2. The repump interaction is taken to be sufficiently effective in returning excited state population to the ground state that only the Raman transition $1 \rightarrow 3$ takes place. The reverse transition $3 \rightarrow 1$ may therefore be neglected. It is further assumed that the repump transitions are excited at a 1-photon detuning of $\Delta_{Laser} \equiv \omega_{12} - \omega_1 = \Delta_{Stokes} + \Delta_F$, to avoid heating from 1-photon interactions. For simplicity, the laser linewidth is taken to match the transition linewidth. For the Ce^{3+} model, the transition rate is then given by the standard expression [19,20]:

$$\Gamma_R(\Delta_{laser}) = \frac{8\pi^3\Gamma_{13} < n >}{\hbar^4[(\delta-\Omega)^2 + i\Gamma_{13}]^2} |\langle f|M|i\rangle|^2, \tag{3}$$

where $< n >$ is the mode occupation number. In this model the summation over intermediate states in the interaction matrix element $\langle f|M|i\rangle$ reduces to a single term with

$$\langle f|M|i\rangle = \left[\frac{\langle 3|\mu^{(e)}\cdot\hat{e}_2|2\rangle\langle 2|\mu^{(e)}\cdot\hat{e}_1|1\rangle}{[\Delta_{Laser} + i\Gamma_{12}]}\right]\frac{E(\omega_1)E\times(-\omega_2)}{4} \tag{4}$$

The duration of excitation is implicitly assumed to be much shorter than the ${}^2F_{7/2}$ lifetime.

For the purpose of illustration, each of the counter-propagating Raman beams is assumed to consist of 1 W focused to a diameter of 300 μm, yielding an average intensity of $I = 2.829 \times 10^3$ W/cm^2 which is comparable to that of Ref. [14]. The refractive index of undoped YAG is $n = 1.8329$ at 575 nm [21]. Other parameters estimated from Fig. 3 and tabulated energy levels [22] are $\Delta_{Laser} = 8.76 \times 10^{14}$ rad/s, $\omega_1 = 3.28 \times 10^{15}$ rad/s, and $\omega_2 = 2.87 \times 10^{15}$ rad/s. The wavevector determined by these optical frequencies is $q = 2.05 \times 10^5$ cm^{-1}, which would correspond to a longitudinal acoustic phonon frequency of $\Omega = 1.77 \times 10^{11}$ rad/s in YAG [21]. However we chose to consider the Raman-active A_{1g} mode of the optical branch [23,24] with a frequency of 783 cm$^{-1} \leftrightarrow 1.885 \times 10^{13}$ rad/s to exploit its higher energy. The dipole moments on the 4f–5d and 5d–4f transitions were presumed to be equal, because the initial and final states are of very similar character. For linear polarization, the squares are proportional to the inverse lifetime τ^{-1} of the 5d state according to

$$|\mu_{12}^{(e)}|^2 \cong |\mu_{23}^{(e)}|^2 = \frac{3\pi c^3\hbar\varepsilon_0}{n\omega^3\tau} \tag{5}$$

Next it is assumed that $\Delta_{Laser} \gg \Gamma_{12}$ and that the initial phonon occupation has the value given in the classical limit. Hence the linewidth may be ignored in $\langle f|M|i\rangle$ and $< n > \cong k_BT/\hbar\Omega \sim 1$. Propagation of the selected phonon causes the bichromatic optical field, which is red-detuned with respect to the ${}^2F_{5/2}(n) \rightarrow {}^2F_{7/2}(n)$ electronic transition, to be "Doppler-shifted" into exact resonance. That is, the transition ${}^2F_{5/2}(n) \rightarrow {}^2F_{7/2}(n-1)$ is fully resonant when $\delta = \Omega$. Upon replacement of field amplitudes with corresponding intensity factors using $I = n\varepsilon_0 cE^2/2$, the expression for the stimulated Raman transition rate reduces to

$$\Gamma_R(\Delta_{laser}) = \frac{8\pi^3}{\hbar^2\omega_1^3\omega_2^3\Gamma_{13}}\left(\frac{3\pi c^2}{n_1 n_2 \tau \Delta_{Laser}}\right)^2 I^2, \tag{6}$$

ignoring pump depletion. The measured lifetime of the 5d state in YAG is $\tau=60$ ns [25]. At room temperature the full width at half maximum of the A_{1g} mode has a value of 12.5 cm^{-1} [24]. Thus, the Raman transition rate is $\Gamma_R(\Delta_{laser})=2.33\ s^{-1}$. Using Eq. (6) in Eq. (2), one finds the initial rate of energy loss per Ce ion at room temperature is

$$R=3.63\times10^{-20}\mathrm{W} \tag{7}$$

For an arbitrarily specified density of Ce ions of $N=10^{21}\ cm^{-3}$, the cooling power within the cylindrical volume illuminated by the beam (namely $V=7.07\times10^{-4}\ cm^3$) in a 1 cm thick sample is then

$$P_{cool}=NV\Gamma_R\hbar\Omega=12.8\,\mathrm{mW} \tag{8}$$

When pulsed with a duty cycle of 50% due to beam-switching, the cooling power would be 6.4 mW for an efficiency of $\eta_{cool}\equiv P_{cool}/P_{in}=0.0128/2\approx0.6\%$. This value begins to approach efficiencies reported in recent experiments based on anti-Stokes fluorescent cooling [14], but uses only a single pass Raman interaction. In Yb-doped media used for anti-Stokes cooling such as Yb:YAG, the intrinsic lifetime of the fluorescent manifold is 0.951 ms [26]. This yields a maximum excitation rate of $1.052\times10^3\ s^{-1}$ per ion whereas the excitation and Raman cooling rate in Ce ions can in principle be pushed much higher due to the short 5d lifetime. The improvement offered by the Raman process over anti-Stokes fluorescent cooling is ascribable to the rapidity (wide bandwidth) of the Raman and repump transitions in combination with the precise interrogation of phonons via the long-lived (narrowband) $^2F_{7/2}$ shelving state of Ce.

The estimate in Eq. (7) is the cooling rate per Ce ion based on interrogation of a fixed frequency optical mode at a high initial temperature. It does not take into account the temperature dependence of quantities such as phonon occupation, linewidths or shifts in the dominant phonon frequency as the sample cools. These effects, as well as the underlying premise that the sample temperature has adequate time to equilibrate with the cooled Raman mode during the irradiation sequence, and that the Ce phonon spectrum is the same as the host bulk modes, are considered next.

4. Temperature dependence, selection rules, and local modes

At low temperatures, the phonon occupation in Eq. (3) drops below one and varies as $<n>\cong\exp(-\hbar\Omega/k_BT)$. In this non-classical regime, Raman cooling might be expected to become ineffective, because the proportionality of Γ_R to $<n>$ appears to reduce the cooling rate dramatically as the temperature drops. However the phonon-broadened linewidth Γ_{13} of the Raman transition in the denominator of Eq. (6) offsets the strong temperature dependence of the numerator with a matching proportionality to $<n>$. With the assumption that linewidth is well-approximated by a fixed, low temperature limit plus a 2-phonon Orbach process [27], it can be modeled as $\Gamma_{13}(T)\cong\Gamma_0(1+\langle n\rangle[\Gamma_0'/\Gamma_0])$. With the further assumption that the phonon-related linewidth parameter Γ_0' is larger than Γ_0, this reduces to $\Gamma_{13}(T)\cong<n>\Gamma_0'$. Upon substitution into Eq. (3), the cooling rate is then predicted to be constant over the entire range $k_BT>\hbar\Gamma_0$, provided Raman resonance is maintained.

This temperature-independent cooling rate is quite different from that obtained with anti-Stokes fluorescence. In the latter case, the phonon-assisted absorption responsible for cooling drops exponentially at low temperatures whereas the background impurity absorption responsible for unintended heating remains constant. This leads to a minimum attainable temperature in the anti-Stokes approach that is relatively high, even in purified solids [28]. The temperature limit applicable to Raman cooling is much lower, and is similar to the Doppler cooling limit in gases $k_BT\approx\hbar\Gamma_0$. For example, in solids with a low temperature inhomogeneous linewidth of $\Gamma_0/2\pi=1$ GHz, the minimum temperature is found to be 48 mK. Thus, the Raman technique offers exponential improvement over the anti-Stokes cooling rate in the cryogenic temperature range, and can attain much lower temperatures.

The one-dimensional Raman interaction described in earlier sections involved a phonon near the center of the Brillouin zone propagating along a single optical axis. However zone center phonons cannot participate directly in the collisional processes that establish thermal equilibrium within the phonon distribution. Hence it is natural to inquire as to how effectively a mode that is cooled irreversibly can equilibrate with the reservoir of other phonons in the solid. Restoration of equilibrium in solids is governed by Umklapp processes, phonon collisions requiring a reciprocal lattice vector $\overline{G}$ to conserve the momentum (see for example [29]). Zone center phonons have low wavevectors, so when two phonons interact with a third via an Umklapp process, there is no way to satisfy the relation $\overline{k}_1+\overline{k}_2=\overline{k}_3+\overline{G}$ with a wavevector $\overline{G}$ that spans the entire Brillouin zone. To achieve uniform cooling of even a single mode, phonons propagating along orthogonal axes should be addressed, and this calls for the introduction of two more sets of counter-propagating Raman beam pairs to cover all three orthogonal space axes. Additionally, beam switching along each axis is needed to interrogate both forward- and backward-travelling phonons of the same frequency. Fast directional switching of each beam pair can be implemented with a Pockel's cell that reverses the propagation direction of the ω_1 and ω_2 beams simultaneously within the sample [16] on a timescale much shorter than the lifetime of the $^2F_{7/2}$ shelving state.

While uniform cooling of one mode can be assured by such procedures, thermal equilibration of the sample as a whole relies on Umklapp processes that involve phonons of wavevector $\overline{G}$. Although the occupation probability of such phonons drops exponentially with decreasing temperature, the thermal conductivity which is proportional to phonon mean free path actually rises through most of the cryogenic ranges. Hence sample equilibration times drop until temperatures around 10–20 K are reached. Then the mean free path becomes limited by sample dimensions and thermal conductivity drops as T^3 due to its proportionality to specific heat [29]. The consequence of this is that fast thermal equilibration can be anticipated in Raman laser-cooling of solids at all but the very lowest ($T<10$ K) temperatures.

In Sections 2 and 3, impurity vibrational modes were implicitly taken to be either the same as those of the host lattice or to be strongly coupled to them. However in dilute crystals, impurity vibrations typically form local modes that differ in frequency and are only weakly coupled to bulk optical modes. As a consequence, the use of stoichiometric crystals for Raman cooling is preferable to doped crystals, to ensure that the local modes are the same as the bulk modes. A suitable host in which the Ce vibrational modes are identical to the bulk modes of the crystal is CeF_3. The density of trivalent Ce ions is much higher in CeF_3 ($N=1.882\times10^{22}\ cm^{-3}$) than in the numerical example for Ce:YAG (see for example [30]), so the laser cooling rate has the potential of being higher. However, at power levels and sample dimensions of the earlier example, pump depletion becomes an issue in CeF_3 and higher incident powers would be needed to achieve optimal efficiency.

5. Conclusion

Two-photon transitions ($4f^n$–$4f^n$) and incoherent pumping on fast transitions ($4f^n$–$4f^{n-1}5d$) of RE^{3+} ions can be combined in an efficient scheme for laser cooling of solids. Narrowband intra-configurational transitions are suitable for selective interactions

with vibrational modes and broadband inter-configurational transitions permit rapid recycling of coolant ions. A key feature of the cooling method outlined here is the identification of a minimum detuning that avoids phonon generation during configuration relaxation or repump operations. Incident light must be detuned to a wavelength on 1-photon transitions that is longer than the longest wavelength of fluorescence from the emitting 5d state. This condition makes it possible to exploit ions with arbitrarily large Stokes shifts for rapid cooling.

The cooling power at room temperature for a single-pass Raman interaction on an optical mode of Ce^{3+}:YAG is predicted to approach that of anti-Stokes cooling of Yb^{3+}:$LiYF_4$ augmented by an enhancement cavity [14]. A limitation of the method is that direct coupling to bulk phonon modes is assured only in stoichiometric crystals like CeF_3. However, the Raman method offers exponential improvement over the cooling power of anti-Stokes fluorescence down to a temperature in the vicinity of $T \approx \hbar\Gamma_0/k_B$. Consequently, the Raman method should make it possible to attain sub-Kelvin temperatures starting from ambient conditions. It is also not restricted to the use of low incident powers as in experiments to date on $4f^n \leftrightarrow 4f^n$ transitions in rare earths. The saturation intensity of $4f^n \leftrightarrow 4f^{n-1}$ 5d transitions like that of Ce^{3+} in CeF_3 is over four orders of magnitude higher than those of resonant transitions in Yb^{3+}. Hence cooling of solids at very high rates with efficiencies on the order of 10% should be feasible throughout the cryogenic range.

Acknowledgment

The author thanks William Meyer for providing the data of Fig. 3. S.C.R. acknowledges helpful discussions with M. Hehlen and support by the Fulbright Foundation that instigated this research.

References

[1] P. Lett, R. Watts, C. Westbrook, W.D. Phillips, P. Gould, H. Metcalf, Phys. Rev. Lett. 61 (1988) 169.
[2] S. Chu, Science 253 (1991) 861.
[3] C. Cohen-Tannoudji, Phys. Rep. 219 (1992) 153.
[4] M.H. Anderson, J.R. Ensher, M.R. Matthews, C.E. Wieman, E.A. Cornell, Science 269 (1995) 198.
[5] C.A. Regal, M. Geiner, D.S. Lin, Phys. Rev. Lett. 92 (2004) 040403.
[6] T.W. Hansch, A.L. Schawlow, Opt. Commun. 13 (1975) 68.
[7] E.L. Raab, M. Prentiss, A. Cable, S. Chu, D.E. Pritchard, Phys. Rev. Lett. 59 (1987) 2631.
[8] J. Dalibard, C. Cohen-Tannoudji, J. Opt. Soc. Am. B2 (1985) 1707.
[9] J. Dalibard, C. Cohen-Tannoudji, J. Opt. Soc. Am. B6 (1989) 2023.
[10] P.J. Ungar, D.S. Weiss, E. Riis, S. Chu, J. Opt. Soc. Am. B6 (1989) 2058.
[11] S. Bowman, N.W. Jenkins, S.P. O'Connor, B.J. Feldman, IEEE J. Quantum Electronics 38 (2002) 1339.
[12] P.F. Cohadon, A. Heidmann, M. Pinard, Phys. Rev. Lett. 83 (1999) 3174.
[13] T. Carmon, Private communication 〈http://arxiv.org/abs/1106.2582〉.
[14] D.V. Seletskiy, S.D. Melgaard, S. Bigotta, A. Di Lieto, M. Tonelli, M. Sheik-Bahae, Nat. Photonics Lett. 4 (2010) 161.
[15] X. Ruan, S.C. Rand, M. Kaviany, Phys. Rev. B 75 (2007) 214304.
[16] J. Reichel, F. Bardou, M.B Dahan, E. Peik, S. Rand, C. Salomon, C. Cohen-Tannoudji, Phys. Rev. Lett. 75 (1995) 4575.
[17] M. Lindberg, J. Javanainen, J. Opt. Soc. Am. B3 (1986) 1008.
[18] R. Gupta, C. Xie, S. Padua, H. Batelaan, H. Metcalf, Phys. Rev. Lett. 71 (1993) 3087.
[19] R. Loudon, Proc. R. Soc. London A 275 (1361) (1963) 218.
[20] Y.R. Shen, The Principles of Nonlinear Optics, J. Wiley & Sons, New York, 1984, p. 143.
[21] L.G. DeShazer, S.C. Rand, B.A. Wechsler, Laser crystals, in: M.J Weber (Ed.), Handbook of Laser Science and Technology, 5, CRC Press, Boca Raton, Florida, 1987, p. 314.
[22] G.M. Williams, N. Edelstein, L.A. Boatner, M.M. Abraham, Phys. Rev. B40 (1989) 4143.
[23] J.P. Hurrell, S.P.S. Porto, I.F. Chang, S.S. Mitra, R.P. Bauman, Phys. Rev. 173 (1968) 851.
[24] Y.F. Chen, P.K. Lim, S.J. Lim, Y.J. Yang, L.J. Hu, H.P. Chiang, W.S. Tse, J. Raman Spectrosc. 34 (2003) 882.
[25] V. Babin, M. Kink, Y. Maksimov, K. Nejezchleb, M. Nikl, S. Zazubovich, J. Lumin. 122–123 (2007) 332.
[26] D. Sumida, T.Y. Fan, Opt. Lett. 19 (1994) 1343.
[27] A. Abragam, B. Bleaney, Electron Paramagnetic Resonance of Transition Ions, Dover Publications, New York, 1970 pp.560–562.
[28] M. Sheik-Bahae, R.I. Epstein, Nat. Photonics 1 (2007) 693.
[29] C. Kittel, Introduction to Solid State Physics, 4th edition, Wiley, New York, 1971 228.
[30] R.C. Weast (Ed.), Handbook of Chemistry and Physics, 49th ed., The Chemical Rubber Company, 1968, B-189.